Original Research

Protective Effects of Neuron-Derived Quiescin Sulfhydryl Oxidase 1 Protein on Intracerebral Hemorrhage

Qi Yao[1], Chenlong Li[1,2], Shengjun Niu[2,3], Siying Chen[2], Jian Chen[1], Suyan Chang[2], Qianqian Liu[1], Gaochao Song[1], Riyun Yang[2,3,]*, Jianhong Shen[1,]*

[1]Department of Neurosurgery, Affiliated Hospital of Nantong University, 226001 Nantong, Jiangsu, China
[2]Medical Morphology Laboratory, Medical School of Nantong University, 226001 Nantong, Jiangsu, China
[3]Department of Histology and Embryology, Medical School of Nantong University, 226001 Nantong, Jiangsu, China
*Correspondence: yangriyunyx@126.com (Riyun Yang); tysjh@163.com (Jianhong Shen)
Academic Editor: Lin-Hua Jiang

Abstract

Background: Intracranial hemorrhage (ICH) poses a serious risk to human health. The shift between pro-inflammatory (M1) and anti-inflammatory (M2) microglial phenotypes is a complex dynamic process. Quiescin sulfhydryl oxidase 1 (QSOX-1) plays a role in protecting cells from damage caused by oxidative stress and in cellular remodeling processes. This study explored how neuron-derived QSOX-1 protein influences the shift in microglial polarization between the M1 and M2 states, and its subsequent impact on nerve function after ICH. **Methods**: QSOX-1 expression in the ICH mouse model was detected. Neuroinflammation, nerve damage, microglial phenotype, nerve function changes, and related signaling pathways were observed in mouse or cell models treated with QSOX-1. **Results**: After ICH, mass spectrometry analysis identified 353 differential proteins, of which the key role of QSOX-1 was verified by bioinformatics analysis. QSOX-1 in the ICH model was highly expressed in the neurons. After treatment with recombinant QSOX-1, the ICH model exhibited reduced neuroinflammation and nerve damage, improved nerve function, and a shift in microglia towards predominantly anti-inflammatory (M2) phenotypes. *In vitro*, QSOX-1 intervention led to reduced inflammation and neuronal cell death. When QSOX-1 expression was upregulated in microglia, the cells primarily shifted towards the M2 phenotype. This shift was accompanied by reduced levels of phosphorylated nuclear factor kappa B (NF-kB) and thioredoxin (TRX)-interacting protein (TXNIP)/NLR family pyrin domain containing 3 (NLRP3) protein, along with increased levels of phosphorylated inhibitor of NF-kB alpha (IkB-α) and TRX. **Conclusion**: Neuron-derived QSOX-1 protein reduces neuroinflammation and promotes nerve function recovery after ICH by regulating microglia phenotype changes, which may be related to the IkB-α/NF-kB and TRX/TXNIP/NLRP3 axis.

Keywords: quiescin sulfhydryl oxidase 1; intracerebral hemorrhage; inhibitor of nuclear kappa B alpha (NF-kB)/NF-kB signaling pathway; thioredoxin (TRX)/TRX-interacting protein/NLR family pyrin domain containing 3 signaling pathway; neuroinflammation; microglia

1. Introduction

Intracranial hemorrhage (ICH) has the characteristics of high mortality, high morbidity, and high recurrence rate, and poses a serious risk to human health. An increasing number of studies have found that neuroinflammation is closely related to the occurrence and development of injuries [1–10]. Therefore, current research on treating ICH is focusing on regulating neuroinflammation to minimize damage to nerve cells.

In the context of pathological conditions like traumatic brain injury, stroke, and multiple sclerosis, researchers have observed inflammatory cell infiltration accompanied by the release of numerous cytokines [11–17]. Microglia, which are among the earliest-appearing non-neuronal cells involved in innate immunity, are primarily categorized into two functional types: pro-inflammatory M1 phenotype and anti-inflammatory M2 phenotype. Microglial M1/M2 polarization is critical for regulating immune responses and host defense mechanisms. Following ICH, this M1/M2 switch becomes a complex dynamic process. Understanding and effectively modulating this polarization remains a significant challenge and are a key focus in current microglial research. Studies have shown that after ICH, various cell types including astrocytes, oligodendrocytes, T cells, and microglia can engage in intercellular communication or crosstalk, which in turn alters the polarization state of the microglia [18–21]. After ICH occurs, ruptured blood vessels release substances like hemoglobin, heme, and iron into the brain parenchyma. These leaked materials are foreign to the brain parenchyma and trigger neurotoxic reactions in the surrounding cells. Neurons exhibit greater sensitivity to hemoglobin or heme than glial cells, and preferentially absorb these specific hemoglobin breakdown products [22]. We hypothesize that complex communication and mutual regulation exist between neurons and microglia after ICH. Despite this potential significance, there is a lack of research investigating the crosstalk between these two cell types after an ICH event.

While microglial polarization is a well-established driver of ICH pathology, the upstream regulators that determine this polarization remain incompletely understood. Quiescin sulfhydryl oxidase 1 (QSOX-1) is a crucial thiol oxidase that plays key roles in disulfide bond formation, oxidative stress regulation, and extracellular matrix assembly [9,10]. In central nervous system (CNS) tumors like glioblastoma and neuroblastoma, upregulation of QSOX-1 drives key aggressive behaviors including tumor cell proliferation, migration, and invasion [15,23]. Despite its established role in promoting CNS tumor progression, the role of QSOX-1 in neuroinflammatory diseases such as ICH and its impact on microglial M1/M2 polarization remain unknown. This study explored the effects of neuron-derived QSOX-1 protein on neuroinflammation and nerve function after ICH and investigated the related mechanisms.

2. Methods

2.1 Animals

C57BL/6 mice and neonatal mice were purchased from the Experimental Animal Center of Nantong University (Jiangsu, China). All animal experiments were conducted according to Animal Research: Reporting of *In Vivo* Experiments (ARRIVE) guidelines. All animal experiments were approved by the Institutional Animal Care & Use Committee of Nantong University. Mice were anesthetized with 3% isoflurane and subsequently euthanized with carbon dioxide (CO_2). The CO_2 concentration was continuously increased until both respiratory and cardiac arrest were confirmed, after which a normal supply of oxygen was provided. The mice achieved loss of consciousness without experiencing pain because the 30–70% CO_2 fill rate was fast enough to guarantee a humane process. The total intervention time for the CO_2 procedure was 50S min.

2.2 Preparation of C57BL/6 Mouse Autologous ICH Model

C57BL/6 male mice weighing 20–25 g were secured in a prone position on a stereotaxic apparatus and kept anesthetized with 3% isoflurane for the duration of the surgery. The cranial top was kept level, and the area around the anterior fontanelle was prepared for skin disinfection. The scalp was cut along the midsagittal line, and the muscle and periosteum were carefully separated to expose the skull. About 30 µL of autologous blood was collected from the tail vein and immediately injected into a specific location (0.2 mm in front of the bregma, 2.3 mm lateral to the midline, and 3.5 mm deep) using a syringe pump at a rate of 2 µL/min. After injecting 5 µL, the process was suspended for 7 min, after which the remaining blood was injected at the same rate. The procedure concluded with a 10 min hold to prevent blood backflow.

2.3 Analysis of Tissue Proteomic Profiles by Label-Free Mass Spectrometry

Briefly, brain tissues from the ICH model were lysed and combined with lysis buffer (4% [w/v] sodium dodecyl sulfate, 100 mM Tris/HCl, pH 7.6, 0.1 M DTT), followed by incubation at 95 °C for 5 min and centrifugation at 14,000 g for 15 min. The protein concentration of the lysate was determined by the Bicinchoninic Acid (BCA) assay. An appropriate amount of protein was taken from each sample for trypsin digestion using the Filter proteome preparation method, and the peptide fragments were desalted using the C18 Cartridge. After lyophilization, the peptide fragments were reconstituted in 40 µL of 0.1% formic acid solution. Each sample was separated using the EasynLC high-performance liquid chromatography system (Thermo Fisher Scientific, Waltham, MA, USA). The samples were chromatographically separated and analyzed with a Q-Exactive mass spectrometer (Thermo Fisher Scientific). Data were analyzed using MaxQuant software (Max Planck Institute of Biochemistry, Martinsried, Germany).

2.4 Bioinformatics Analysis

Gene Ontology (GO) functional enrichment and Kyoto Encyclopedia of Genes and Genomes (KEGG) pathway analysis were used to analyze the differential genes. The network of differentially expressed proteins was analyzed for its protein–protein interactions (PPIs). The above bioinformatics analyses were performed by clusterProfile software (version 4.8.3; Cluster 3.0; Stanford University, Stanford, CA, USA). Through the above analysis, the molecular target QSOX-1 of this study was identified.

2.5 C57BL/6 Mouse Autologous ICH Model Was Treated With Recombinant QSOX-1 Protein

The *in vivo* study sample sizes were calculated based on statistical power and a predetermined effect size. C57BL/6 male mice (20–25 g) were randomly divided into the following three groups based on random numbers generated using Statistics Package for Social Science (SPSS) software (version 28, IBM, Chicago, IL, USA): (1) The sham group underwent mock surgery (craniotomy without blood infusion) followed by treatment with 0.1 mL 0.9% saline; (2) The ICH+vehicle group underwent autologous ICH surgery followed by treatment with 0.9% saline; and (3) The ICH+ recombinant QSOX-1 (rQSOX-1) group received an injection of rQSOX-1 into the ipsilateral lateral ventricle (1 µg/µL, 50 µg/kg) 30 min after autologous ICH surgery, followed by a second injection 24 h later. The drug concentrations used were determined in preliminary experiments (**Supplementary Fig. 1**). The mice in the ICH+vehicle group were treated with the same dose of solvent (sterile saline). In a separate group of 24 C57BL/6 mice (sham group), the animals underwent all aspects of the model protocol (anesthesia, skin incision, and craniotomy)

with the exception of autologous blood injection, and were treated with the same dose of solvent. On postoperative days 1, 3, 5, 7, and 14, 24 mice per group were anesthetized, and fresh brains were collected and frozen in liquid nitrogen for later use.

2.6 Analysis of the Therapeutic Effects of rQSOX-1 Protein on the ICH Model

The wet-to-dry ratios (WDRs) were used to analyze the brain edema as previously described [24]. Wet brain tissues were weighed and heated in a drying oven at 100 °C for 3 days, after which the dry brain tissues were weighed. Tissue water content was calculated using the formula: $(1 - \text{dry weight} / \text{wet weight}) \times 100\%$. The neurologic deficits of the ICH mice were assessed with modified neurologic severity scores (mNSS) as previously described [25,26]. The higher the score, the more severe the neurologic deficits. The locomotion function of mice was detected by the CatWalk gait analysis method as described by Hamers et al. [27] and Koopmans et al. [28]. The locomotion parameters of interest in the ICH model were as follows: Print area, Max area, Pressure, Swing, Swing speed, Duty cycle, Stride length, Base of support, Cadence, Average speed of the hind paw, and forepaw. The mice were analyzed using the CatWalk apparatus (Noldus Information Technology, Wageningen, The Netherlands), and the paw print footage was analyzed automatically with the CatWalk computer program (Noldus Information Technology).

2.7 M1 Phenotype-Induced Differentiation Culture

Six neonatal mice (P1 or P2) were purchased from the Experimental Animal Center of Nantong University. After removing the scalp and skull, the brain tissue was extracted and the cortex was isolated for the preparation of microglial cells. The resulting mixed glial cells were initially cultured for approximately 12–14 days in conditioned medium containing 10% fetal bovine serum (FBS) and 1% penicillin-streptomycin. Then microglia cells were detached from the mixed glial cells in an incubator at 37 °C at 200 rpm. The purity of the resulting microglia was greater than 95%. The M1 phenotype differentiation of microglia cells used four distinct groups for comparison: control, rQSOX-1, lipopolysaccharide (LPS), and LPS+rQSOX-1 groups. Microglial cells in the control group were cultured in Dulbecco's Modified Eagle Medium (DMEM) containing 10% FBS; cells in the rQSOX-1 group were cultured in DMEM containing 10% FBS and 50 nM rQSOX-1; cells in the LPS group were cultured in DMEM containing 10% FBS and 100 ng/mL LPS; and cells in the LPS+rQSOX-1 group were cultured in DMEM containing 10% FBS, 100 ng/mL LPS, and 50 nM rQSOX-1. Microglial cells were seeded in 96-well plates at a density of 1.5×10^5 cells/well. After 7 days of culture, cells were collected for flow cytometry analysis, and culture medium was collected for enzyme-linked immunosorbent assay (ELISA) analysis. The drug con-

centrations used were obtained in preliminary experiments (**Supplementary Fig. 2**).

2.8 Co-Culture of Neurons and Microglia Cells

Six neonatal mice (P1 or P2) were purchased from the Experimental Animal Center of Nantong University. The scalp and skull were incised to expose the brain, and the cortex was harvested. Cortical tissue was enzymatically digested with 0.125% trypsin at 37 °C for 15 min, followed by gentle trituration to achieve a single-cell suspension, which was filtered and centrifuged. The supernatant was discarded, and the cell pellet was resuspended in 3 mL of 10% FBS/DMEM. The cell concentration was determined by counting, and the cells were subsequently cultured in flasks. Neurons were cultured in 10% FBS/DMEM at 37 °C in a humidified chamber with 95% air and 5% CO_2. Half of the medium was changed every 2 days. The neurons were used for further research when they covered about 90% of the flask.

Transwell culture was used to co-culture the neurons and microglia cells. The transwell culture was divided into four groups: control, rQSOX-1, LPS, and LPS+rQSOX-1 groups. The control group received only media; the rQSOX-1 group received 50 nM rQSOX-1; the LPS group received 100 ng/mL LPS; and the LPS+rQSOX-1 group received combined treatment of 100 ng/mL LPS and 50 nM rQSOX-1. The co-culture groups were prepared by seeding neurons into the lower chambers in 10% FBS/DMEM containing 50 nM mouse hemoglobin. Microglial cells were seeded into the corresponding upper chambers in 10% FBS/DMEM and treated as follows: the control group received only media; the rQSOX-1 group received 50 nM rQSOX-1; the LPS group received 100 ng/mL LPS; and the LPS+rQSOX-1 group received combined treatment of 100 ng/mL LPS and 50 nM rQSOX-1. After 7 days of culture, neurons were collected for flow cytometry analysis.

2.9 Cell Transfection and Transcriptome Analysis

Microglial cells were cultured in a 6-well culture plate at a concentration of 5×10^3 cells/mL. After 24 h, they were transfected with the QSOX-1 overexpression vector (pcDNA-QSOX-1; Shanghai Sun Biotech Co., Ltd., Shanghai, China) using Lipofectamine 2000 (Thermo Fisher Scientific) according to the manufacturer's instructions. The transfected cells were placed in an incubator set to 37 °C with 5% CO_2. A blank control group was included in the experiment. After 48 h, the transfected cells underwent transcriptome analysis (Shanghai Genechem Co., Ltd., Shanghai, China). The stably transfected microglia M1 phenotype-induced differentiation experiments with LPS were divided into four groups: control vector, LPS+vector, QSOX-1 vector, and LPS+QSOX-1 vector groups. In the control vector group and LPS+vector group, microglia transfected with an empty vector were cultured. In the QSOX-1 vector group and LPS+QSOX-1 vec-

tor group, microglia transfected with empty QSOX-1 vector were cultured. After 7 days of culture, cells were collected for Western blot and culture medium was collected for ELISA.

2.10 Flow Cytometry Analysis

Flow cytometry was used to detect microglia phenotype or neuronal apoptosis according to a previous study [29]. The antibodies or cell stains were as follows: Fluorescein Isothiocyanate (FITC)-labeled anti-cluster of differentiation 86 (CD86), Allophycocyanin (APC)-labeled anti-CD206, Phycoerythrin (PE)-labeled anti-CD11b, PE-Cyanine7-labeled anti-CD45, and an Annexin V Apoptosis Detection Kit. Cells were gated to sequentially exclude debris [Forward Scatter-Area (FSC-A) vs. Side Scatter-Area (SSC-A)] and doublets (FSC-H vs. FSC-A). Live cells were identified as Annexin V-Enhanced Green Fluorescent Protein (EGFP) and propidium iodide Propidium Iodide (PI)-negative. Microglia (CD11b+ CD45 low) were distinguished from peripheral macrophages (CD11b+ CD45 high). The resulting microglia population was then assessed for M1 (CD86+) and M2 (CD206+) phenotypes. Analysis was performed using the Fluorescence-Activated Cell Sorting (FACS) Calibur flow cytometer with Cell Quest software (BD Biosciences, Franklin Lakes, NJ, USA).

2.11 Quantitative PCR Analysis

Quantitative PCR (qPCR) was performed using a protocol as previously described [30]. The sense and antisense primers were synthesized as follows: GAPDH 5′-TCCCT CAAGATTGTCAGCAA-3′, 5′-AGATCCACAACGGAT ACATT-3′; QSOX-1 5′-GACTTCCCATCTTGTTAC-3′, 5′-CCGAAGATAGGATGTATAG-3′; TXNIP 5′-CGAG TCAAAGCCGTCAGGAT-3′, 5′-CGTTCTCACCTGCT GTAGGC-3′, TRX 5′-CTCATCCAGAAGTTTGGGGAC C-3′, 5′-GTTGTTCTTCACGTCCAGCAG-3′, NLRP3 5′-AGGCTGCTATCTGGAGGAACT-3′, 5′-GCAACGGAC ACTCGTCATCT-3′.

2.12 Western Blot Analysis

Western blot was performed as previously described [30]. The primary antibodies used were as follows: rabbit anti-QSOX-1 (1:800; Abcam, Cambridge, UK), rabbit anti-CD206 (M2 marker, 1:800; Thermo Fisher Scientific), rabbit anti-CD86 (M1 marker, 1:800; Thermo Fisher Scientific), rabbit anti-thioredoxin (TRX) (1:800; Abcam), rabbit anti-thioredoxin-interacting protein (TXNIP) (1:800; Thermo Fishers Scientific), rabbit anti-NLR family pyrin domain containing 3 (NLRP3) (1:800; Thermo Fisher Scientific), rabbit anti-nuclear factor kappa B (NF-kB) (1:800; Abcam), rabbit anti-phosphorylated NF-κB (p-NF-kB) (1:800; Abcam), rabbit anti-p-NF-kB (1:800; Abcam) rabbit anti-inhibitor of NF-kB alpha IkB-α (1:800; Abcam), and rabbit anti-p-IkB-α (1:800; Abcam). After primary antibody incubation, they were incubated with the horseradish peroxidase-conjugated goat anti-rabbit secondary antibody (1:1000; Abcam) and visualized using the enhanced chemiluminescence system (Pierce, Rockford, IL, USA). In addition, GAPDH or β-actin was used as a reference protein.

2.13 Immunohistochemistry and Immunofluorescence

For immunohistochemistry, the tissue slides were incubated with rabbit anti-QSOX-1 (1:800; Abcam) at room temperature for 1 h. Antibody binding was detected using diaminobenzidine. For immunofluorescence, the tissue slides or cells were incubated with the following primary antibodies: rabbit anti-QSOX-1 (1:600; Abcam), mouse anti-NeuN (neuronal marker, 1:600; Abcam), mouse anti-glial fibrillary acidic protein (glial cell marker, 1:800; Abcam), mouse anti-ionized calcium-binding adaptor molecule 1 (Iba-1) (microglia marker, 1:800; Abcam), rabbit anti-CD206 (1:600; Thermo Fisher Scientific), and rabbit anti-inducible nitric oxide synthase (iNOS) (M1 marker, 1:600; Thermo Fisher Scientific). The secondary antibodies used were: Alexa Fluor® 568 labeled goat anti-rabbit secondary antibody (1:1000; Abcam) and Alexa Fluor® 488 labeled goat anti-mouse (1:1000; Abcam) secondary antibody. Finally, cell nuclei were counter-stained with DAPI (5 µg/mL; Abcam). The positive cells were observed under a fluorescence microscope (Leica, Wetzlar, Germany) at 400× magnification.

2.14 ELISA

The levels of tumor necrosis factor alpha (TNF-α), interleukin 10 (IL-10), IL-1β, and IL-14 in the medium of each group were measured using the corresponding ELISA detection kit (Beyotime, Beijing, China) according to the manufacturer's instructions.

2.15 Cell Viability/Cytotoxicity Detection

Neuron viability and death level *in vitro* were detected with the Calcein-AM·PI Kit (Thermo Fisher Scientific) according to the manufacturer's instructions. Fluorojade B (FJB) staining was used to assess the level of neuron death *in vivo* (Millipore, Burlington, MA, USA) according to the manufacturer's instructions.

2.16 Statistical Analyses

The numbers of repeated samples or mice are listed in the figure legends. To address the multiple testing problem inherent in high-throughput transcriptomic data, we applied a correction for multiple comparisons. The raw *p*-values obtained from the differential expression tests were adjusted using the Benjamin-Hochberg procedure to control the false discovery rate (FDR). Genes with an adjusted *p*-value (FDR) <0.05 were considered statistically significant. Statistical analyses were performed using SPSS Statistics 21.0. The measurement data in this study were found to follow a normal distribution, as determined by the Kolmogorov-Smirnov test, and are presented as the mean
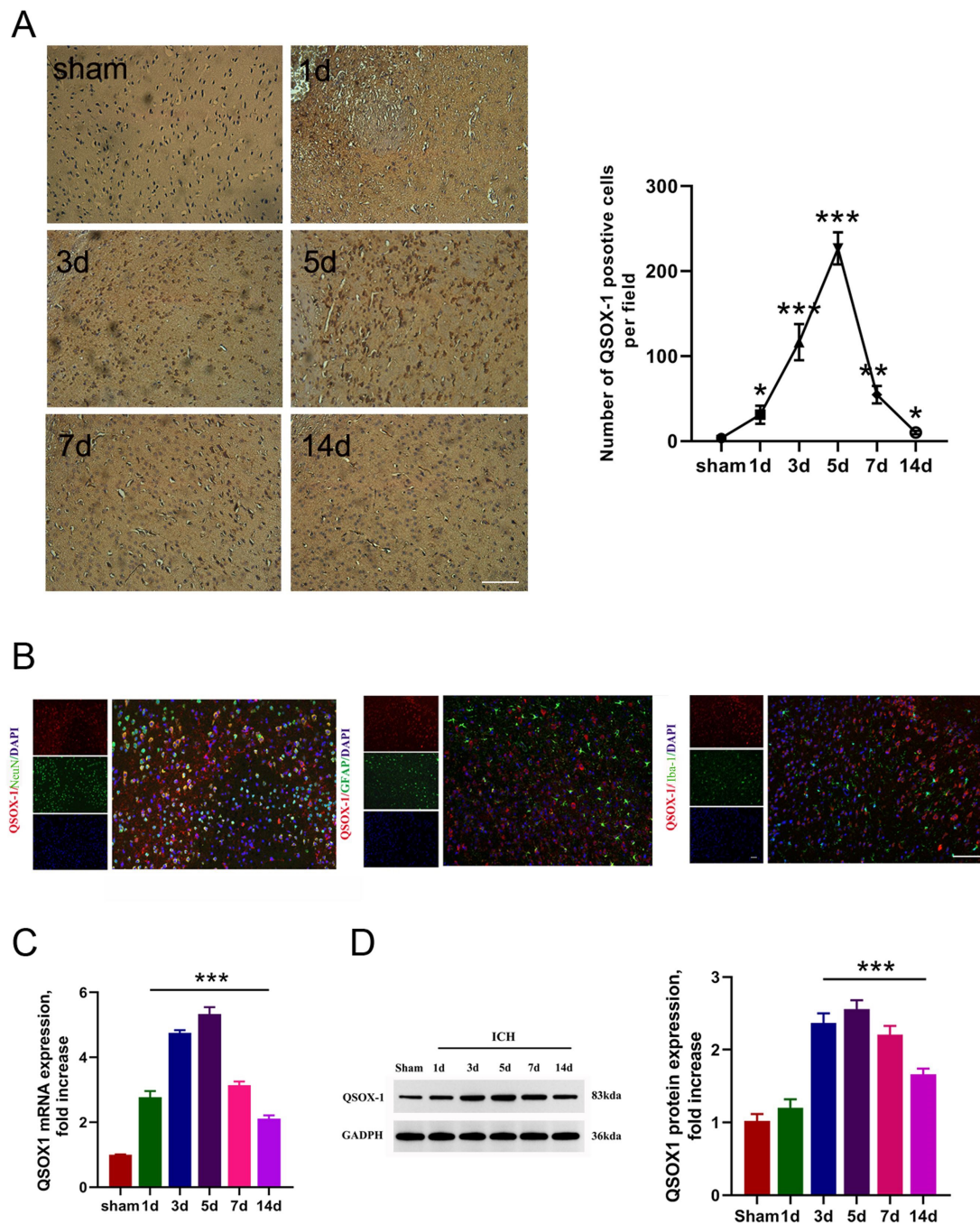
Fig. 1. QSOX-1 protein was highly expressed in the ICH mouse model. (A) QSOX-1 protein expression was detected by immuno-histochemistry (n = 4 mice, four sections per mouse). Scale bar: 200 μm. (B) Immunofluorescence results showed that QSOX-1 protein was mainly expressed in neurons (n = 4 mice, four sections per mouse). Scale bar: 200 μm (the original image), Scale bar: 160 μm (the enlarged image). (C) QSOX-1 mRNA expression was detected by RT-PCR (n = 4 experimental replicates). (D) QSOX-1 protein expression was detected by Western blot analysis and was consistent with the immunohistochemistry results (n = 4 experimental replicates). * vs. sham, $p < 0.05$; ** vs. sham, $p < 0.01$; *** vs. sham, $p < 0.001$ (independent t-test). QSOX-1, quiescin sulfhydryl oxidase 1; ICH, intracranial hemorrhage.

± standard deviation. Group comparisons were conducted using an independent t-test or one-way analysis of variance. $p < 0.05$ was considered statistically significant.

3. Results

3.1 Differential Protein Expression After ICH

The results of label-free mass spectrometry (MS) showed a total of 353 differential proteins, of which 99 were
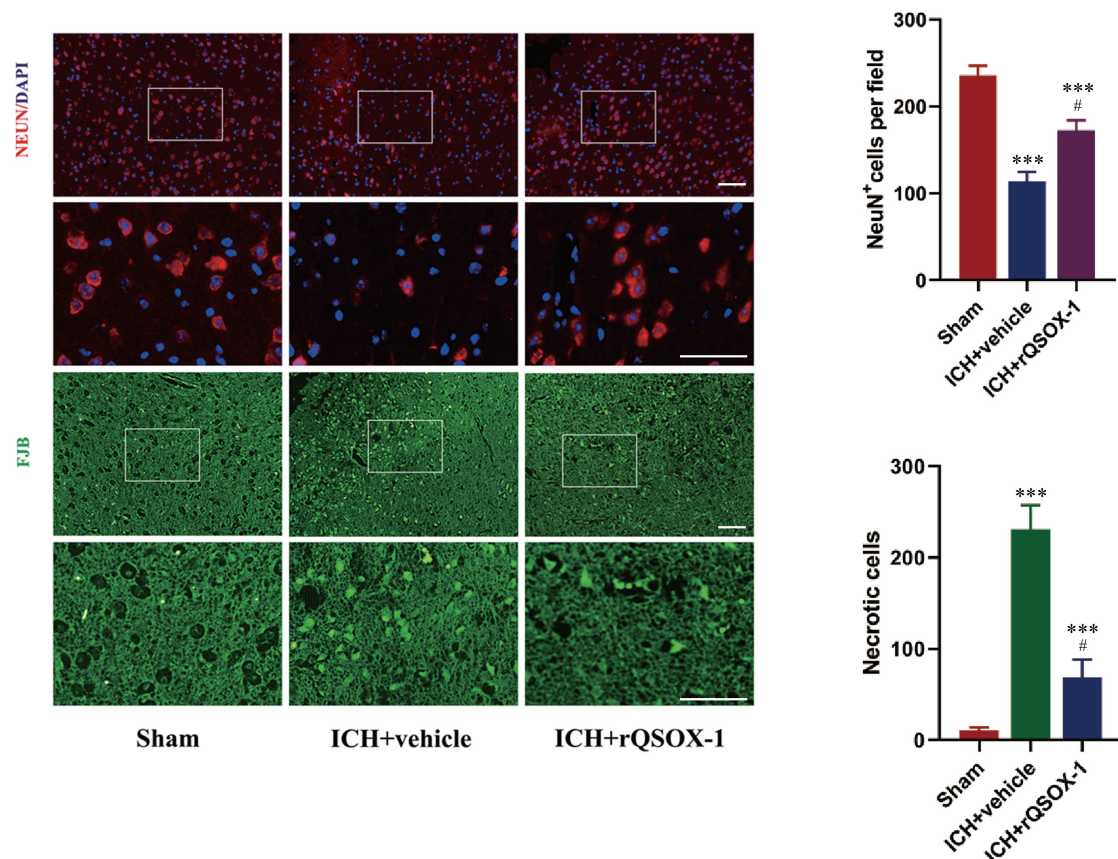
Fig. 2. Immunofluorescence results showed that the QSOX-1 protein was mainly expressed in neurons (n = 4 mice, four sections per mouse). Scale bar: 222 µm (the original image), Scale bar: 200 µm (the enlarged image). *** vs. sham, $p < 0.001$; # vs. ICH+vehicle, $p < 0.05$ (one-way analysis of variance).

upregulated and 254 were downregulated; QSOX-1 protein was identified as being upregulated (**Supplementary Fig. 3A**). GO function and KEGG pathway analysis showed that the functions of these differentially expressed proteins were mainly binding, catalytic activity, molecular function regulator, transporter activity, and structural molecule activity. These differentially expressed proteins were mainly involved in cellular processes, biological regulation, regulation of biological processes, and important metabolic biological processes such as process and cellular component organization or biogenesis (**Supplementary Fig. 3B**). PPI analysis showed that QSOX-1 protein played a key role (**Supplementary Fig. 3C**), and the above analysis identified QSOX-1 as a molecular target.

3.2 QSOX-1 Protein is Highly Expressed in the ICH Mouse Model

Immunohistochemistry results revealed a significant increase in QSOX-1-positive cells within the brain tissue of mice in the ICH model group compared to the sham group. Specifically, levels were increased on day 1, remained elevated on day 3, peaked on day 5, and gradually decreased from day 7 through day 14; however, even on day 14, levels remained higher than those observed in the sham group (Fig. 1A). The findings from Real-Time polymerase chain reaction (RT-PCR) and Western blot experiments were consistent with the results of immunohistochemistry analysis (Fig. 1C,D). Immunofluorescence results showed that QSOX-1 protein was mainly expressed in neurons (Fig. 1B).

3.3 rQSOX-1 Treatment Decreases Nerve Damage Levels and Increases Nerve Function In Vivo

Immunofluorescence results showed that NeuN-positive cells in the ICH+vehicle and ICH+rQSOX-1 groups were significantly decreased compared with the sham group. In addition, the ICH+rQSOX-1 group exhibited more NeuN-positive cells than the ICH+vehicle group. Both the ICH+vehicle and ICH+rQSOX-1 groups showed significant increases in FJB-positive cells compared to the sham group, but the number of FJB-positive cells in the ICH+rQSOX-1 group was lower than that of the ICH+vehicle group (Fig. 2).

The results of WDR analysis showed that the water content in the affected brain hemisphere was significantly elevated in both the ICH+vehicle group and ICH+rQSOX-1 group compared with the sham group. However, the water content was lower in the ICH+rQSOX-1 group than in
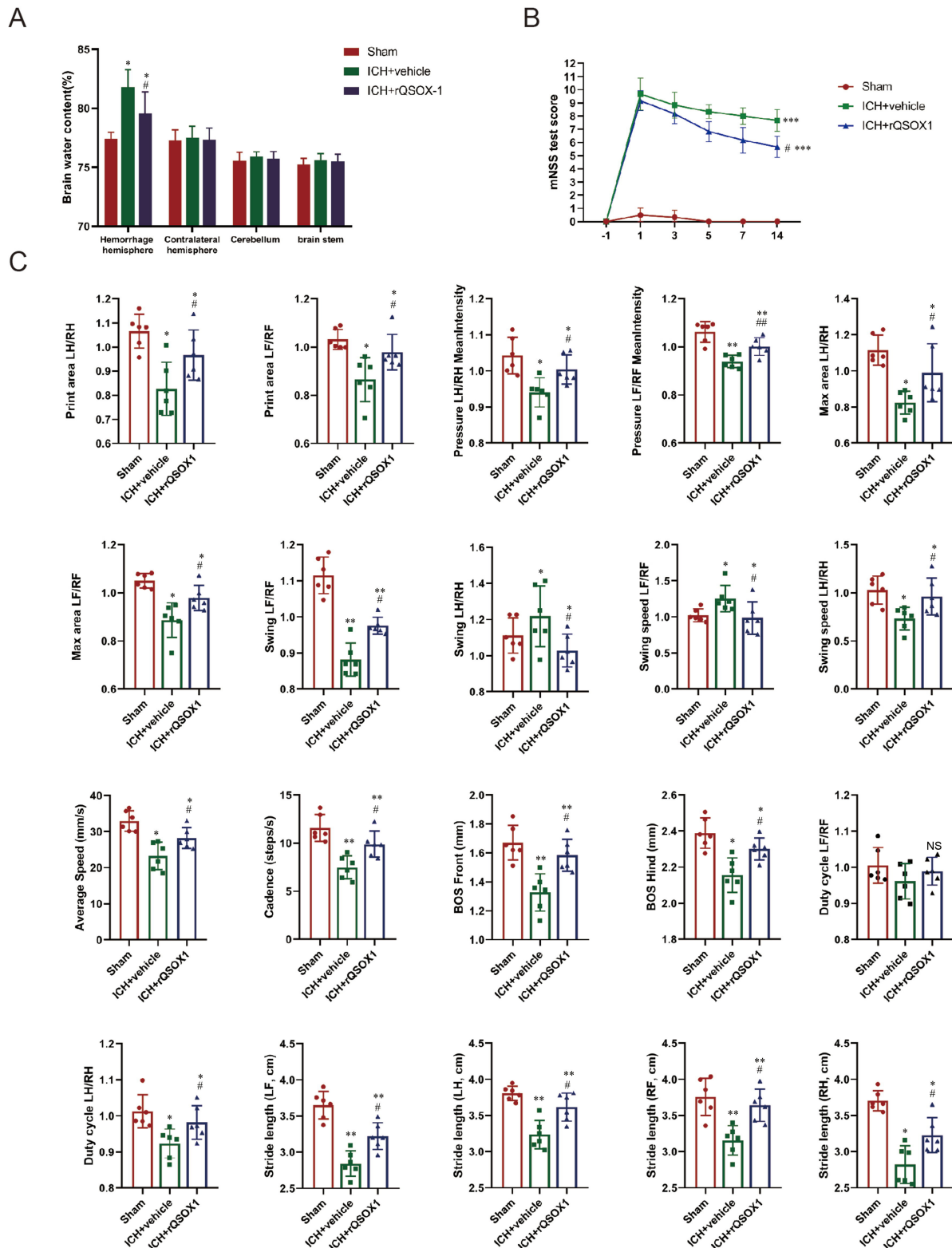
Fig. 3. rQSOX1 treatment reduces brain water content and enhances neurobehavioral outcomes following ICH. (A) The brain water content was assessed by WDR (n = 6 mice/group). (B) The neurologic deficits of the ICH mice were assessed with mNSS (n = 6 mice/group). (C) The locomotion function of mice was detected by CatWalk gait analysis (n = 6 mice/group). LH, left hind paw; LF, left forepaw. RH, right hind paw; RF, right forepaw. * vs. sham, $p < 0.05$; ** vs. sham, $p < 0.01$; # vs. ICH+vehicle, $p < 0.05$; ## vs. ICH+vehicle, $p < 0.01$; NS vs. ICH+vehicle, $p > 0.05$ (one-way analysis of variance).

the ICH+vehicle group (Fig. 3A), indicating that rQSOX-1 treatment reduced swelling compared to vehicle treatment. The mNSS results showed that mNSS changes were minimal in the sham group, with scores remaining near zero. Compared to the sham group, both the ICH+vehicle and ICH+rQSOX-1 groups exhibited significantly increased mNSS on days 1, 3, 5, 7, and 14. mNSS in the ICH+rQSOX-1 group were consistently lower than those in the ICH+vehicle group. mNSS in the ICH+vehicle and ICH+rQSOX-1 groups showed a gradual downward trend, and the decline in the ICH+rQSOX-1 group was more obvious (Fig. 3B). CatWalk gait analysis showed that the Print area, Max area, Pressure, Swing, Swing speed, Duty cycle, Stride length, Base of support, Cadence, Average speed of hind paw and forepaw were worse in the ICH+vehicle and ICH+rQSOX-1 groups compared with the sham group. The ICH+rQSOX-1 group demonstrated better outcomes in these measurements than the ICH+vehicle group (Fig. 3C).

3.4 rQSOX-1 Promotes M2 Microglial Differentiation

In the sham group, there were minimal numbers of both M2 phenotype (CD206/Iba-1 double-positive) cells and M1 phenotype (INOS/Iba-1 double-positive) cells. Following ICH, the ICH+vehicle group showed significant increases in both M1 and M2 cell types. However, after treatment with rQSOX-1, the population of M2 phenotype cells increased while the number of M1 phenotype cells decreased (Fig. 4A). Flow cytometry analysis showed that CD206 fluorescence intensity significantly increased and CD86 fluorescence intensity significantly decreased after rQSOX-1 treatment (Fig. 4B).

In an *in vitro* study of M1 microglia differentiation induced by LPS, the application of rQSOX-1 protein resulted in a significant increase in fluorescence intensity of the CD206 marker and a significant decrease in fluorescence intensity of the CD86 marker, as revealed by flow cytometry analysis (Fig. 5A). ELISA showed that LPS stimulation caused M1 polarization, as evidenced by significant increases in IL-1β and TNF-α levels and significant decreases in IL-10 and IL-4 levels in the medium. Treatment with rQSOX-1 protein reversed this trend: IL-1β and TNF-α levels significantly decreased, while IL-10 and IL-4 levels significantly increased (Fig. 5B). *In vitro*, following transfection of microglia with QSOX-1 vector, a significant increase in QSOX-1 mRNA levels was observed (Fig. 5C). QSOX-1 overexpression significantly promoted the expression of CD206 while simultaneously inhibiting the expression of CD86 (Fig. 5D). Furthermore, ELISA results indicated that QSOX-1 overexpression significantly enhanced IL-10 expression levels and inhibited IL-1β and TNF-α expression levels.

3.5 Protective Effect of rQSOX-1 Treatment on Neurons In Vitro

In the co-culture of neurons and microglia cells, neuron damage was induced by hemoglobin, while microglia cells were stimulated with LPS (Fig. 6A). Flow cytometry analysis showed high rates of neuronal apoptosis, and cell viability/cytotoxicity detection showed a significant number of PI-positive cells with only a few Calcein-AM-positive cells. Treatment with rQSOX-1 protein effectively mitigated this damage, leading to a significant decrease in neuronal apoptosis and the number of PI-positive cells, and a notable increase in Calcein-AM-positive cells (Fig. 6B,C).

3.6 Transcriptome Analysis and Preliminary Analysis of Signaling Pathways

After QSOX-1 overexpression, transcriptome analysis showed inhibition of various pro-inflammatory signaling pathways in microglia, including NF-kB, Toll-like receptor, IL-17, TNF, Janus kinase (JAK)/signal transducer and activator of transcription (STAT), necroptosis, NOD-like receptor, and cytokine–cytokine interactions (Fig. 7A–C). The protein most significantly suppressed was TXNIP (Fig. 7D). Western blot analysis corroborated these findings, demonstrating that QSOX-1 overexpression led to decreased levels of p-NF-kB and TXNIP/NLRP3, while levels of p-IkB-α and TRX increased (Fig. 8A,B). As shown in Fig. 9A–C, the functions of rQSOX-1 treatment were reversed by the overexpression of TXNIP.

4. Discussion

In this study, we found that neuron-derived QSOX-1 promoted the microglia M2 polarization switch, reduced neuroinflammation, and promoted nerve function recovery after ICH. Studies have shown that QSOX1 is involved in protecting cells from oxidative stress and facilitating cellular remodeling [31,32]. In this study, brain tissues in the ICH model were analyzed by label-free MS. The results showed that QSOX-1 protein expression was upregulated, and PPI analysis showed that QSOX-1 protein played a key role in the protein interactions. Using an ICH mouse model, the temporal and spatial expression changes in QSOX-1 protein were characterized. The protein's expression surged, reaching peak levels at 5 days after injury, followed by a decrease, while still maintaining a high expression state long-term. Immunofluorescence results confirmed that QSOX-1 protein was mainly expressed in neurons. To explore the role of QSOX-1 protein in ICH, we conducted relevant experiments *in vitro* and *in vivo*. The results of *in vitro* mouse model experiments showed that treatment with QSOX-1 protein significantly decreased nerve damage levels and increased nerve function, indicating that QSOX-1 protein protects against ICH. *In vitro* cell experiments verified the neuroprotective effect of QSOX-1 protein. We found that QSOX-1 protein influences the switch
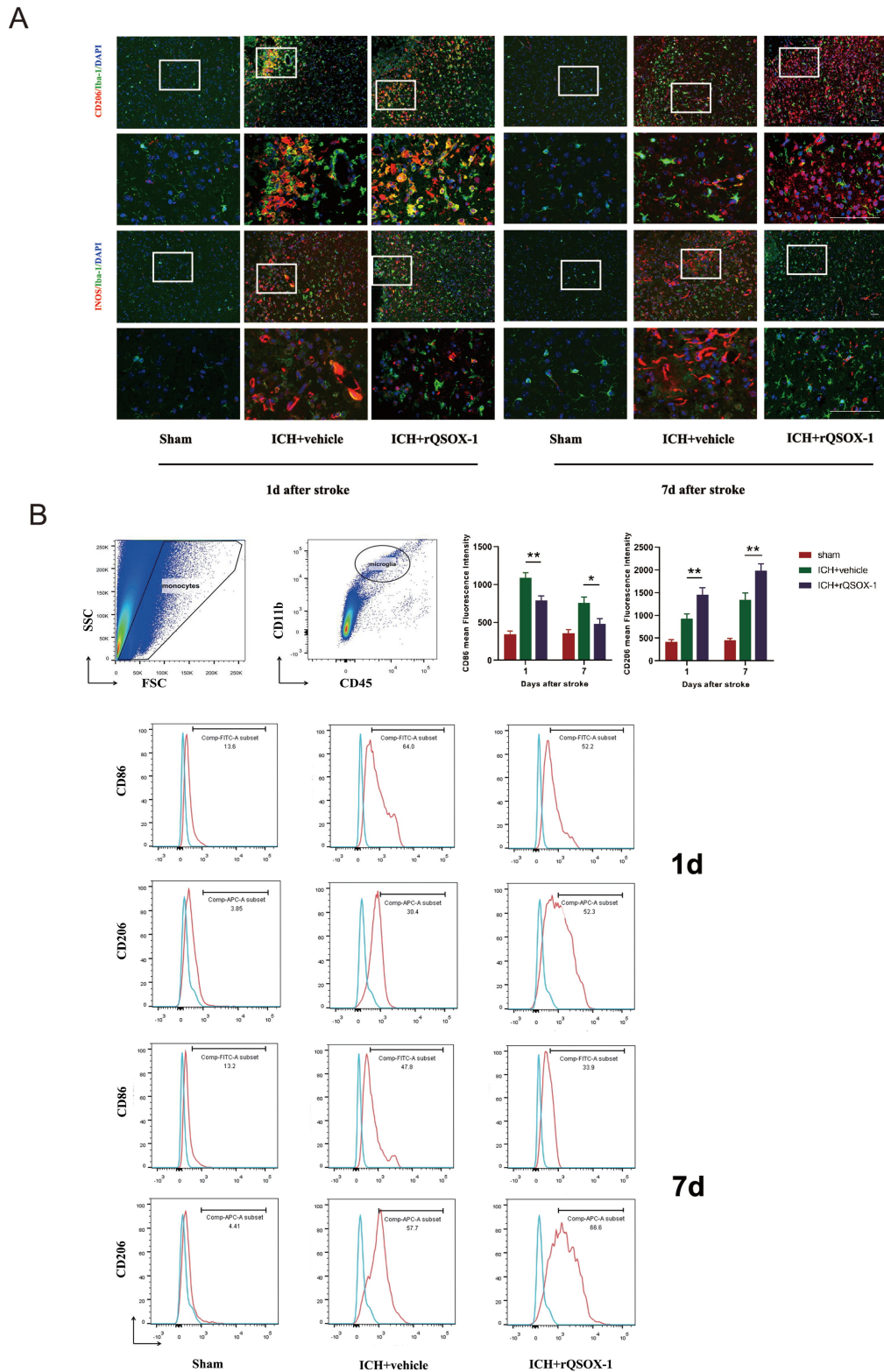
Fig. 4. rQSOX-1 promoted M2 phenotype differentiation of microglia cells. (A) Microglial M1/M2 polarization switch was detected *in vivo* by CD206/Iba-1 and INOS/Iba-1 immunofluorescence (n = 4 mice, four sections per mouse). Scale bar: 500 µm (the original image), Scale bar: 200 µm (the enlarged image). (B) Microglial M1/M2 polarization switch was detected *in vivo* using flow cytometry to quantify CD206 and CD86 fluorescence (n = 4 experimental replicates). * vs. ICH+vehicle, $p < 0.05$; ** vs. ICH+vehicle, $p < 0.01$ (one-way analysis of variance). rQSOX-1, recombinant QSOX-1.
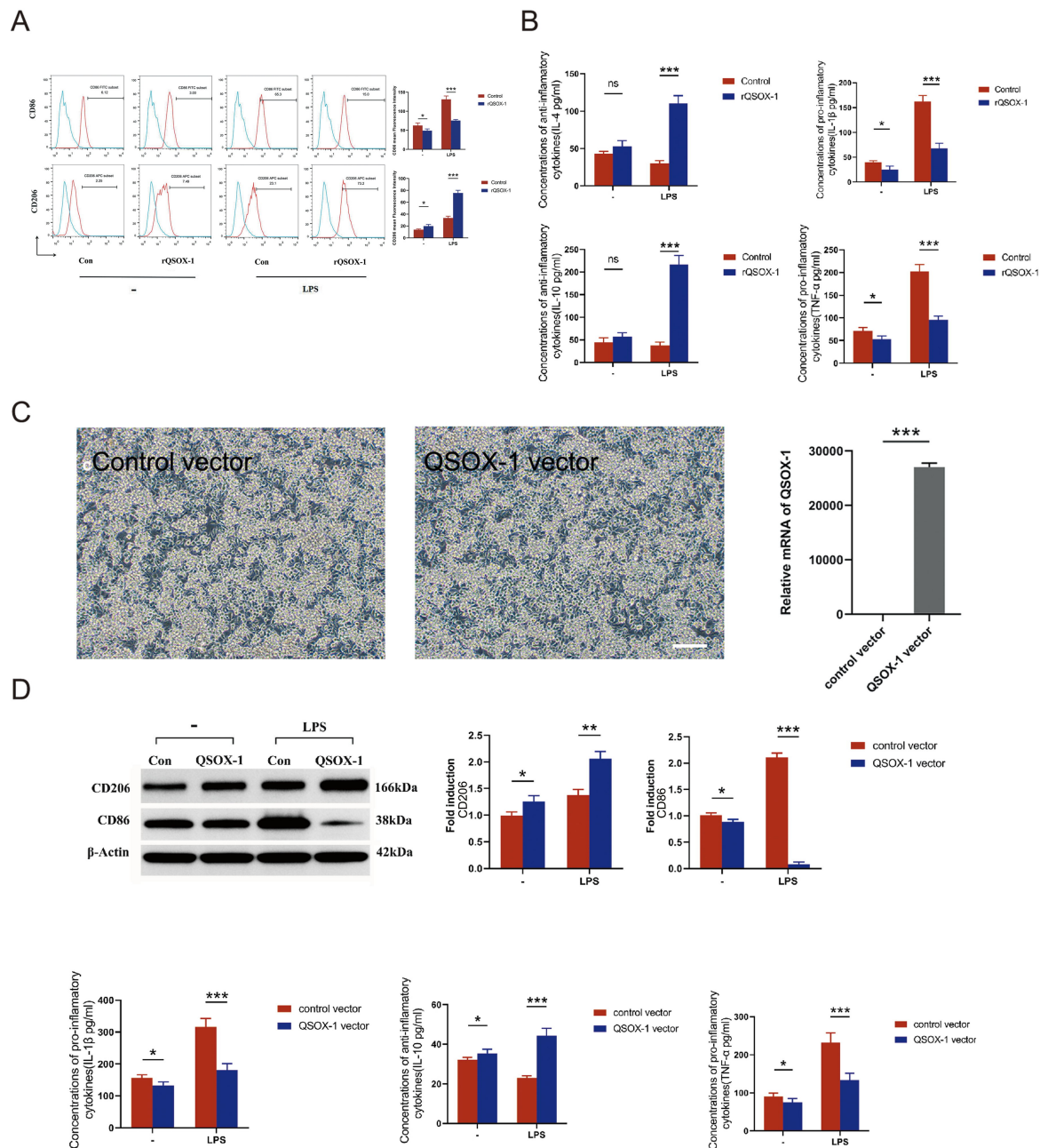
Fig. 5. rQSOX1 promotes an anti-inflammatory phenotype in microglia in vitro. (A) *In vitro*, flow cytometry was used to assess the M1/M2 polarization switch in microglia by measuring the fluorescence intensity of the M2 marker CD206 and M1 marker CD86 (n = 4 experimental replicates). (B) IL-4, IL-10, IL-1β, and TNF-α levels in medium were detected by ELISA (n = 4 experimental replicates). (C) *In vitro*, after microglia were transfected with QSOX-1 vector, the QSOX-1 mRNA levels significantly increasesd (n = 4 experimental replicates) Scale bar: 40 µm. (D) *In vitro*, QSOX-1 overexpression significantly promoted the expression of CD206 and inhibited the expression of CD86, which was verified by Western blotting (n = 4 experimental replicates). ELISA showed that QSOX-1 overexpression significantly upregulated IL-10 expression and inhibited IL-1β and TNF-α expression levels (n = 4 experimental replicates). * vs. control, $p < 0.05$; ** vs. control, $p < 0.01$; *** vs. control, $p < 0.001$; ns vs. control, $p > 0.05$ (an independent *t*-test). IL, interleukin; TNF-α, tumor necrosis factor alpha; ELISA, enzyme-linked immunosorbent assay.

in microglial cell polarization. This was demonstrated *in vitro* and *in vivo* by direct QSOX-1 treatment or overexpression in microglia. The results showed that QSOX-1 promoted the M2 phenotype differentiation of microglia cells.

At the same time, QSOX-1 inhibited the expression of proinflammatory factors and promoted the expression of anti-inflammatory factors. These findings suggest that the protective effect of QSOX-1 on ICH is closely related to its
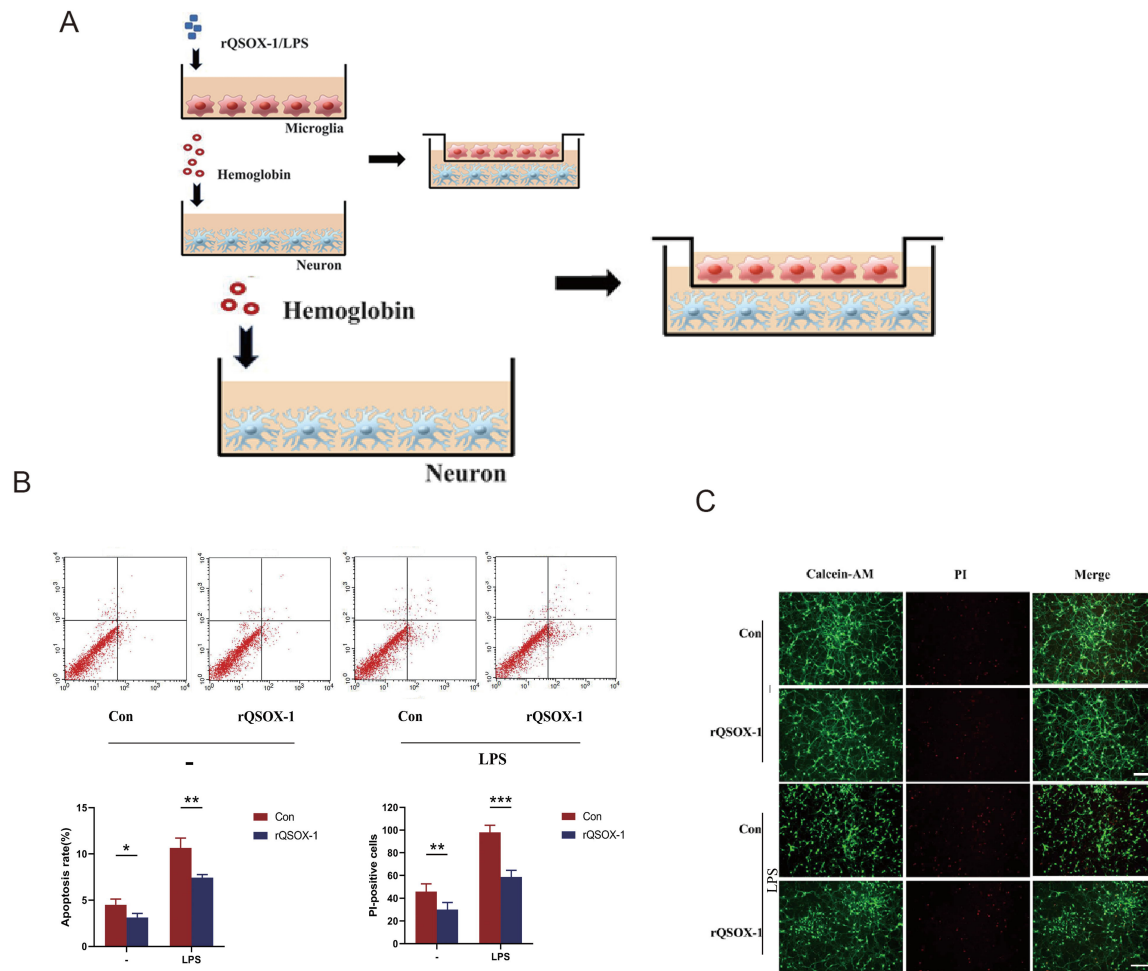
Fig. 6. Protective effect of rQSOX-1 treatment on neurons *in vitro*. (A) In the co-culture of neurons and microglia cells, neuron damage was induced by hemoglobin, while microglia cells were stimulated with LPS. The figure was created with BioRender. (B) The neuronal apoptosis rate was assessed with flow cytometry (n = 4 experimental replicates). (C) The cell viability/cytotoxicity was detected with Calcein-AM and PI staining (n = 4 experimental replicates). Scale bar: 40 μm. * vs. control, $p < 0.05$; ** vs. control, $p < 0.01$; *** vs. control, $p < 0.001$ (independent *t*-test). LPS, lipopolysaccharide.

regulation of M2 phenotype differentiation and inhibition of neuroinflammation. However, the underlying molecular signaling mechanism is still unclear. Therefore, after microglia overexpressed QSOX-1, transcriptome sequencing was performed. The results showed that pro-inflammatory signaling pathways in microglia such as NF-κB, Toll-like receptor, IL-17, TNF, JAK/STAT, necroptosis, NOD-like receptor, and cytokine–cytokine interactions were inhibited, and volcano map showed the TXNIP protein was most significantly suppressed. In this study, NF-κB and TXNIP signaling pathways were selected for preliminary research. This study provides initial evidence indicating that QSOX-1 overexpression induces the transition of microglia to an anti-inflammatory (M2) phenotype via the NF-κB and TXNIP signaling pathways. This finding introduces a novel element to the understanding of post-hemorrhagic brain repair by identifying a previously unrecognized player in microglial polarization. In the broader context of ICH

research, most therapeutic strategies have focused on blood pressure management [33], hematoma evacuation [34], and general immunosuppression [35]. By contrast, our work identifies QSOX-1 as a specific endogenous protein that, upon supplementation, shifts the immune response toward a protective M2 state. Our results both complement and contrast existing work on microglial modulation in ICH. For instance, studies by Yang *et al*. [36] demonstrated that the cytokine IL-4 can promote M2 polarization and improve recovery after ICH, whereas our findings identified QSOX-1 as a non-cytokine factor capable of achieving a similar beneficial shift. More importantly, we have linked this effect to specific downstream signaling axes, the NF-κB and NLRP3 signaling pathways, which are key mediators of neuroinflammation [37,38]. A limitation of this study was that the exploration of the NF-κB and TXNIP signaling pathways was at the correlation level. As a result, we will further explore its mechanism in future studies.
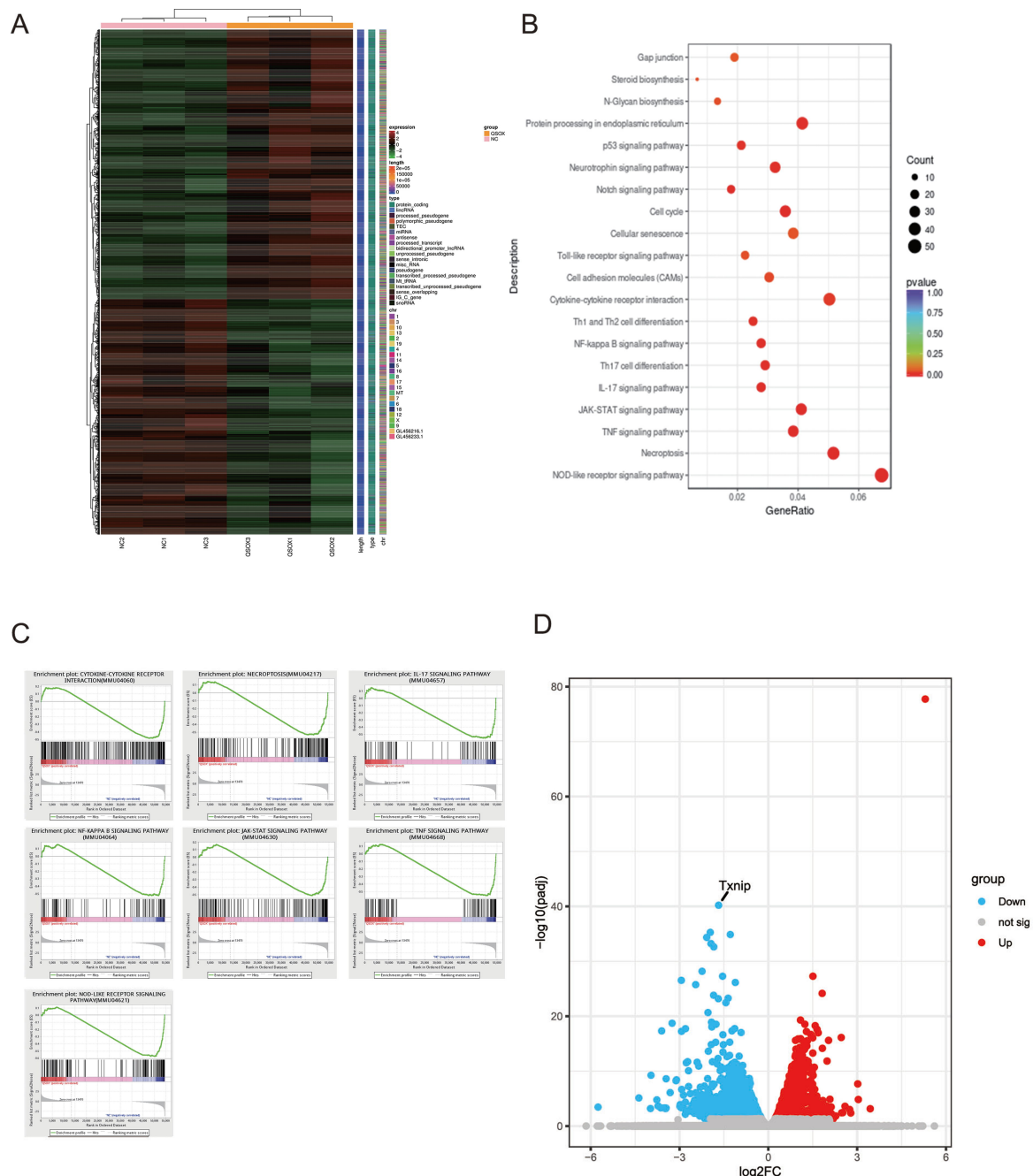
Fig. 7. Transcriptome analysis and preliminary analysis of signaling pathways. (A) Heatmap of differentially expressed genes (DEGs). (B) Gene Ontology (GO) enrichment analysis of DEGs. (C) Gene set enrichment analysis of DEGs. (D) Volcano map showed that the thioredoxin (TRX)-interacting protein (TXNIP) protein was most significantly suppressed.

Pu *et al.* [39] and Liu *et al.* [40] investigated the protective effect and underlying mechanism of silymarin in paraquat-induced macrophage injury and found that silymarin pretreatment significantly reduced cytotoxicity, promoted the expression of TRX and antioxidant enzymes, and inhibited the activation of TXNIP and NLRP3 inflammasomes. Silymarin attenuates paraquat-induced macrophage cytotoxicity by inhibiting oxidative stress, NLRP3 inflammasome activation, cytokine secretion, and apoptosis. Our results showed that QSOX-1 overexpression in the mi-

croglia increased the expression of TRX and inhibited the expression of TXNIP and NLRP3, which may be related to the neuroprotective effects of QSOX-1 against ICH. Studies have shown that NF-κB signaling is closely related to stroke, ischemia-reperfusion injury, neuroinflammation, and microglial polarity switching [41–45]. Liu *et al.* [45] reported that Pterostilbene attenuated astrocytic inflammation and neuronal oxidative injury after ischemia-reperfusion by inhibiting NF-κB phosphorylation. Zhao *et al.* [42] found that the NF-κB pathway promoted mi-
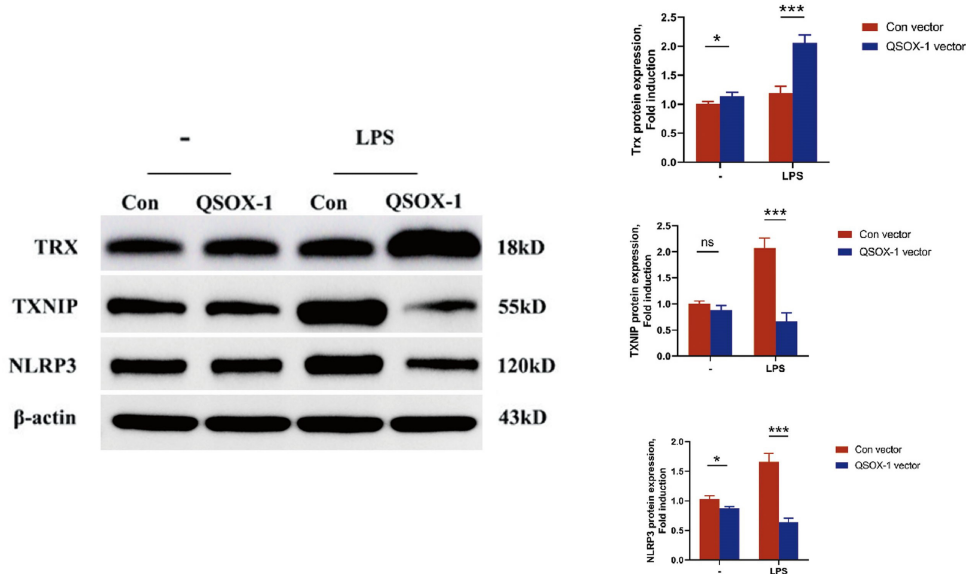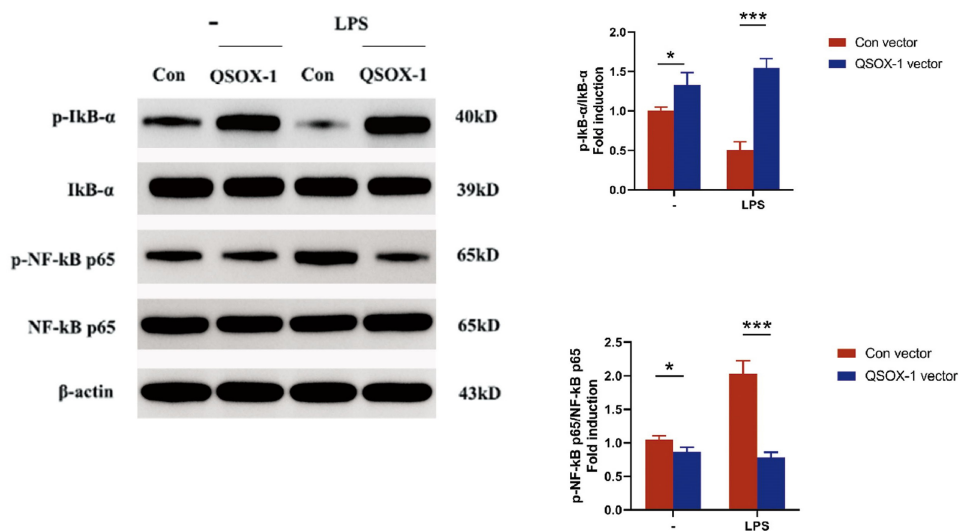
Fig. 8. QSOX-1 overexpression abrogated LPS-induced NLRP3 inflammasome activation and NF-κB signaling. (A) Western blot analysis showed that TXNIP/NLRP3 proteins levels decreased and TRX level increased after QSOX-1 overexpression under the condition of LPS stimulation (n = 4 experimental replicates). (B) Western blot analysis showed p-NF-kB levels decreased and p-IkB-α levels increased after QSOX-1 overexpression (n = 4 experimental replicates). * vs. control vector, $p < 0.05$; *** vs. control vector, $p < 0.001$; ns vs. ICH+vehicle, $p > 0.05$ (independent t-test). NLRP3, NLR family pyrin domain containing 3.

croglia M1 polarization and inhibited microglia polarization toward the M2 phenotype. While the relationship between NF-κB and QSOX-1 has not been previously reported, our study showed that QSOX-1 overexpression in microglia promotes IkB-α phosphorylation, inhibits NF-κB phosphorylation, and drives M2 polarization. Future studies are needed to clarify how QSOX-1 relates to the NF-κB and TXNIP signaling pathways, its effect on microglia phenotype changes, and its direct interaction with key molecules.

Our study presents direct evidence that supplementing the QSOX-1 protein itself can elicit therapeutic effects in a preclinical model of ICH, establishing rQSOX-1 as a promising biologic therapeutic candidate. However, the translation of this intracerebroventricular (ICV) protein delivery approach into a clinically feasible treatment faces significant challenges that must be recognized. Despite the potency of ICV injection as an experimental method, its high invasiveness and associated risks for patients warrant attention. The development of less invasive delivery tech-
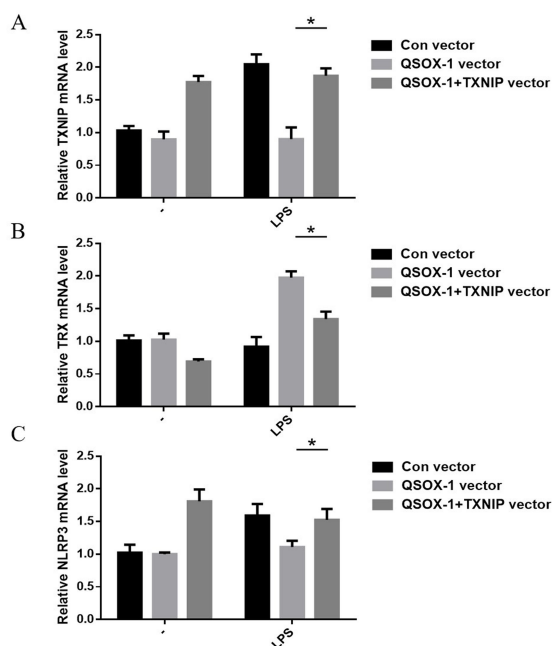
Fig. 9. Overexpression of TXNIP combined with rQSOX-1 treatment. (A) qPCR results showed that the mRNA level of TXNIP was increased in the QSOX-1+TXNIP group compared to the QSOX-1 group. (B) qPCR results showed that the mRNA level of TRX was decreased in the QSOX-1+TXNIP group compared to the QSOX-1 group. (C) qPCR results showed that the mRNA level of NLRP3 was increased in the QSOX-1+TXNIP group compared to the QSOX-1 group (n = 6 experimental replicates). * vs. QSOX-1 vector (independent *t*-test).

niques capable of effectively transporting this large protein across the blood–brain barrier (BBB) is of utmost importance. Future endeavors could investigate engineered BBB-penetrating antibodies, nanoparticle carriers, or intranasal delivery pathways. The pharmacokinetic profile of rQSOX-1 within the brain parenchyma remains unknown. Essential parameters such as its half-life, distribution, and optimal dosing regimen must be meticulously characterized to formulate an efficacious treatment protocol for a dynamic condition like ICH. The immunogenicity and long-term safety implications of administering a recombinant protein into the central nervous system have not been explored comprehensively. Thorough toxicology assessments and immunogenicity studies in clinically relevant models are fundamental prerequisites for progressing to clinical development. While our discoveries illuminate a promising avenue for therapy, they also underscore the extensive translational efforts needed in the future.

5. Conclusions

Our study demonstrates that neuron-derived QSOX-1 plays a crucial protective role in the aftermath of ICH. It effectively mitigates neuroinflammation and neuronal damage, facilitates the transition of microglia toward the anti-inflammatory M2 phenotype, and promotes functional recovery. The underlying mechanism appears to involve modulation of the IkB-α and TRX/TXNIP/NLRP3 signaling pathways. These findings highlight QSOX-1 as a promising therapeutic target for alleviating brain injury and improving recovery following ICH.

Availability of Data and Materials

All data reported in this paper will also be shared by the author Qi Yao (nantongyaoqi@163.com) lead contact upon request.

Author Contributions

JHS, RYY conceived and designed the experiments. QY, CLL, SJN, SYChen, JC, SYChang performed experiments. QQL, GCS analyzed the data. QY wrote the paper. All authors contributed to editorial changes in the manuscript. All authors read and approved the final manuscript. All authors have participated sufficiently in the work and agreed to be accountable for all aspects of the work.

Ethics Approval and Consent to Participate

This study was approved by the Animal Experiment Committee of Nantong University (S20240714-004, S20201018-176). All animal experiments were conducted according to Animal Research: Reporting of *In Vivo* Experiments (ARRIVE) guidelines.

Acknowledgment

We would like to express our gratitude to all those who helped me during the writing of this manuscript. Thanks to all the peer reviewers for their opinions and suggestions.

Conflict of Interest

The authors declare no conflict of interest.

Supplementary Material

Supplementary material associated with this article can be found, in the online version, at https://doi.org/10.31083/FBL45176.

References

[1] Fu Y, Hao J, Zhang N, Ren L, Sun N, Li YJ, *et al*. Fingolimod for the treatment of intracerebral hemorrhage: a 2-arm proof-of-concept study. JAMA Neurology. 2014; 71: 1092–1101. https://doi.org/10.1001/jamaneurol.2014.1065.

[2] Mracsko E, Javidi E, Na SY, Kahn A, Liesz A, Veltkamp R. Leukocyte invasion of the brain after experimental intracerebral hemorrhage in mice. Stroke. 2014; 45: 2107–2114. https://doi.org/10.1161/STROKEAHA.114.005801.

[3] Shao A, Zhu Z, Li L, Zhang S, Zhang J. Emerging therapeutic targets associated with the immune system in patients with intracerebral haemorrhage (ICH): From mechanisms to translation. eBioMedicine. 2019; 45: 615–623. https://doi.org/10.1016/j.ebiom.2019.06.012.

[4] Taylor RA, Sansing LH. Microglial responses after ischemic stroke and intracerebral hemorrhage. Clinical & Developmental Immunology. 2013; 2013: 746068. https://doi.org/10.1155/2013/746068.

[5] Hao H, Yin T, Li T, Zhou X, Ren H, Liu M, *et al*. Inhibition of Bruton's tyrosine kinase restricts neuroinflammation following intracerebral hemorrhage. Theranostics. 2025; 15: 494–508. https://doi.org/10.7150/thno.101024.

[6] Wang DP, Yin H, Lin Q, Fang SP, Shen JH, Wu YF, *et al*. Andrographolide enhances hippocampal BDNF signaling and suppresses neuronal apoptosis, astroglial activation, neuroinflammation, and spatial memory deficits in a rat model of chronic cerebral hypoperfusion. Naunyn-Schmiedeberg's Archives of Pharmacology. 2019; 392: 1277–1284. https://doi.org/10.1007/s00210-019-01672-9.

[7] Li J, Shen S, Shen H. Heat-shock protein A12A attenuates oxygen-glucose deprivation/reoxygenation-induced human brain microvascular endothelial cell dysfunction via PGC-1α/SIRT3 pathway. Drug Development Research. 2024; 85: e22130. https://doi.org/10.1002/ddr.22130.

[8] Zhou B, Wang H, Zhang B, Zhang L. Licochalcone B attenuates neuronal injury through anti-oxidant effect and enhancement of Nrf2 pathway in MCAO rat model of stroke. International Immunopharmacology. 2021; 100: 108073. https://doi.org/10.1016/j.intimp.2021.108073.

[9] Chakravarthi S, Jessop CE, Willer M, Stirling CJ, Bulleid NJ. Intracellular catalysis of disulfide bond formation by the human sulfhydryl oxidase, QSOX1. The Biochemical Journal. 2007; 404: 403–411. https://doi.org/10.1042/BJ20061510.

[10] Ilani T, Alon A, Grossman I, Horowitz B, Kartvelishvily E, Cohen SR, *et al*. A secreted disulfide catalyst controls extracellular matrix composition and function. Science. 2013; 341: 74–76. https://doi.org/10.1126/science.1238279.

[11] Hickman S, Izzy S, Sen P, Morsett L, El Khoury J. Microglia in neurodegeneration. Nature Neuroscience. 2018; 21: 1359–1369. https://doi.org/10.1038/s41593-018-0242-x.

[12] Ponomarev ED, Maresz K, Tan Y, Dittel BN. CNS-derived interleukin-4 is essential for the regulation of autoimmune inflammation and induces a state of alternative activation in microglial cells. The Journal of Neuroscience. 2007; 27: 10714–10721. https://doi.org/10.1523/JNEUROSCI.1922-07.2007.

[13] Sarlus H, Heneka MT. Microglia in Alzheimer's disease. The Journal of Clinical Investigation. 2017; 127: 3240–3249. https://doi.org/10.1172/JCI90606.

[14] Xu W, Huang Y, Zhou R. NLRP3 inflammasome in neuroinflammation and central nervous system diseases. Cellular & Molecular Immunology. 2025; 22: 341–355. https://doi.org/10.1038/s41423-025-01275-w.

[15] Araújo DGB, Nakao L, Gozzo P, Souza CDA, Balderrama V, Gugelmin ES, *et al*. Expression level of quiescin sulfhydryl oxidase 1 (QSOX1) in neuroblastomas. European Journal of Histochemistry. 2014; 58: 2228. https://doi.org/10.4081/ejh.2014.2228.

[16] Kiss MG, Mindur JE, Yates AG, Lee D, Fullard JF, Anzai A, *et al*. Interleukin-3 coordinates glial-peripheral immune crosstalk to incite multiple sclerosis. Immunity. 2023; 56: 1502–1514.e8. https://doi.org/10.1016/j.immuni.2023.04.013.

[17] Li Y, Shen G, Du J, Dai W, Su Z. Neuroprotective Potential of Ethoxzolamide Targeting Oxidative Stress and Inflammation in Experimental Models of Intracerebral Hemorrhage. Frontiers in Bioscience (Landmark Edition). 2024; 29: 356. https://doi.org/10.31083/j.fbl2910356.

[18] de Souza Ferreira LP, da Silva RA, Borges PP, Xavier LF, Scharf P, Sandri S, *et al*. Annexin A1 in neurological disorders: Neuroprotection and glial modulation. Pharmacology & Therapeutics. 2025; 267: 108809. https://doi.org/10.1016/j.pharmthera.2025.108809.

[19] He X, Huang Y, Liu Y, Zhang X, Wang Q, Liu Y, *et al*. Astrocyte-derived exosomal lncRNA 4933431K23Rik modulates microglial phenotype and improves post-traumatic recovery via SMAD7 regulation. Molecular Therapy. 2023; 31: 1313–1331. https://doi.org/10.1016/j.ymthe.2023.01.031.

[20] Gong G, Shao L, Wang Y, Chen CY, Huang D, Yao S, *et al*. Phosphoantigen-activated V gamma 2V delta 2 T cells antagonize IL-2-induced CD4+CD25+Foxp3+ T regulatory cells in mycobacterial infection. Blood. 2009; 113: 837–845. https://doi.org/10.1182/blood-2008-06-162792.

[21] Chen S, Wu H, Klebe D, Hong Y, Zhang J, Tang J. Regulatory T cell in stroke: a new paradigm for immune regulation. Clinical & Developmental Immunology. 2013; 2013: 689827. https://doi.org/10.1155/2013/689827.

[22] Lara FA, Kahn SA, da Fonseca AC, Bahia CP, Pinho JP, Graca-Souza AV, *et al*. On the fate of extracellular hemoglobin and heme in brain. Journal of Cerebral Blood Flow and Metabolism. 2009; 29: 1109–1120. https://doi.org/10.1038/jcbfm.2009.34.

[23] Geng Y, Xu C, Wang Y, Zhang L. Quiescin Sulfhydryl Oxidase 1 Regulates the Proliferation, Migration and Invasion of Human Glioblastoma Cells via PI3K/Akt Pathway. OncoTargets and Therapy. 2020; 13: 5721–5729. https://doi.org/10.2147/OTT.S255941.

[24] Lin TN, He YY, Wu G, Khan M, Hsu CY. Effect of brain edema on infarct volume in a focal cerebral ischemia model in rats. Stroke. 1993; 24: 117–121. https://doi.org/10.1161/01.str.24.1.117.

[25] Otero L, Zurita M, Bonilla C, Aguayo C, Vela A, Rico MA, *et al*. Late transplantation of allogeneic bone marrow stromal cells improves neurologic deficits subsequent to intracerebral hemorrhage. Cytotherapy. 2011; 13: 562–571. https://doi.org/10.3109/14653249.2010.544720.

[26] Chen J, Li Y, Wang L, Zhang Z, Lu D, Lu M, *et al*. Therapeutic benefit of intravenous administration of bone marrow stromal cells after cerebral ischemia in rats. Stroke. 2001; 32: 1005–1011. https://doi.org/10.1161/01.str.32.4.1005.

[27] Hamers FP, Lankhorst AJ, van Laar TJ, Veldhuis WB, Gispen WH. Automated quantitative gait analysis during overground locomotion in the rat: its application to spinal cord contusion and transection injuries. Journal of Neurotrauma. 2001; 18: 187–201. https://doi.org/10.1089/08977150150502613.

[28] Koopmans GC, Deumens R, Honig WMM, Hamers FPT, Steinbusch HWM, Joosten EAJ. The assessment of locomotor function in spinal cord injured rats: the importance of objective analysis of coordination. Journal of Neurotrauma. 2005; 22: 214–225. https://doi.org/10.1089/neu.2005.22.214.

[29] Wang D, Liu F, Zhu L, Lin P, Han F, Wang X, *et al*. FGF21 alleviates neuroinflammation following ischemic stroke by modulating the temporal and spatial dynamics of microglia/macrophages. Journal of Neuroinflammation. 2020; 17: 257. https://doi.org/10.1186/s12974-020-01921-2.

[30] Yao Q, Cai G, Yu Q, Shen J, Gu Z, Chen J, *et al*. IDH1 mutation diminishes aggressive phenotype in glioma stem cells. International Journal of Oncology. 2018; 52: 270–278. https://doi.org/10.3892/ijo.2017.4186.

[31] Sun X, Zheng M, Zhang M, Qian M, Zheng Y, Li M, *et al*. Differences in the expression of chromosome 1 genes between lung telocytes and other cells: mesenchymal stem cells, fibroblasts, alveolar type II cells, airway epithelial cells and lymphocytes. Journal of Cellular and Molecular Medicine. 2014; 18: 801–810. https://doi.org/10.1111/jcmm.12302.

[32] Morel C, Adami P, Musard JF, Duval D, Radom J, Jouvenot M. Involvement of sulfhydryl oxidase QSOX1 in the protection of cells against oxidative stress-induced apoptosis. Experimental Cell Research. 2007; 313: 3971–3982. https://doi.org/10.1016/j.yexcr.2007.09.003.

[33] Lattanzi S, Silvestrini M. Optimal achieved blood pressure in acute intracerebral hemorrhage: INTERACT2. Neurology. 2015; 85: 557–558. https://doi.org/10.1212/01.wnl.0000470918.40985.d0.

[34] Ziai WC, McBee N, Lane K, Lees KR, Dawson J, Vespa P, *et al*. A randomized 500-subject open-label phase 3 clinical trial of minimally invasive surgery plus alteplase in intracerebral hemorrhage evacuation (MISTIE III). International Journal of Stroke. 2019; 14: 548–554. https://doi.org/10.1177/1747493019839280.

[35] Magid-Bernstein J, Girard R, Polster S, Srinath A, Romanos S, Awad IA, *et al*. Cerebral Hemorrhage: Pathophysiology, Treatment, and Future Directions. Circulation Research. 2022; 130: 1204–1229. https://doi.org/10.1161/CIRCRESAHA.121.319949.

[36] Yang J, Ding S, Huang W, Hu J, Huang S, Zhang Y, *et al*. Interleukin-4 Ameliorates the Functional Recovery of Intracerebral Hemorrhage Through the Alternative Activation of Microglia/Macrophage. Frontiers in Neuroscience. 2016; 10: 61. https://doi.org/10.3389/fnins.2016.00061.

[37] Song L, Pei L, Yao S, Wu Y, Shang Y. NLRP3 Inflammasome in Neurological Diseases, from Functions to Therapies. Frontiers in Cellular Neuroscience. 2017; 11: 63. https://doi.org/10.3389/fncel.2017.00063.

[38] Yu H, Lin L, Zhang Z, Zhang H, Hu H. Targeting NF-κB pathway for the therapy of diseases: mechanism and clinical study. Signal Transduction and Targeted Therapy. 2020; 5: 209. https://doi.org/10.1038/s41392-020-00312-6.

[39] Pu Y, Han S, Chen J, Liu Z. MANF inhibits NLRP3 inflammasome activation by competitively binding to DDX3X in paraquat-stimulated alveolar macrophages. Ecotoxicology and Environmental Safety. 2024; 287: 117331. https://doi.org/10.1016/j.ecoenv.2024.117331.

[40] Liu Z, Sun M, Wang Y, Zhang L, Zhao H, Zhao M. Silymarin attenuated paraquat-induced cytotoxicity in macrophage by regulating Trx/TXNIP complex, inhibiting NLRP3 inflammasome activation and apoptosis. Toxicology in Vitro. 2018; 46: 265–272. https://doi.org/10.1016/j.tiv.2017.10.017.

[41] Liu Y, Wang W, Di B, Miao J. Curcumol ameliorates neuroinflammation after cerebral ischemia-reperfusion injury via affecting microglial polarization and Treg/Th17 balance through Nrf2/HO-1 and NF-κB signaling. Cell Death Discovery. 2024; 10: 300. https://doi.org/10.1038/s41420-024-02067-3.

[42] Zhao R, Ying M, Gu S, Yin W, Li Y, Yuan H, *et al*. Cysteinyl Leukotriene Receptor 2 is Involved in Inflammation and Neuronal Damage by Mediating Microglia M1/M2 Polarization through NF-κB Pathway. Neuroscience. 2019; 422: 99–118. https://doi.org/10.1016/j.neuroscience.2019.10.048.

[43] Xie W, Zhu T, Dong X, Nan F, Meng X, Zhou P, *et al*. HMGB1-triggered inflammation inhibition of notoginseng leaf triterpenes against cerebral ischemia and reperfusion injury via MAPK and NF-κB signaling pathways. Biomolecules. 2019; 9: 512. https://doi.org/10.3390/biom9100512.

[44] Zhou X, Zhang YN, Li FF, Zhang Z, Cui LY, He HY, *et al*. Neuronal chemokine-like-factor 1 (CKLF1) up-regulation promotes M1 polarization of microglia in rat brain after stroke. Acta Pharmacologica Sinica. 2022; 43: 1217–1230. https://doi.org/10.1038/s41401-021-00746-w.

[45] Liu H, Wu X, Luo J, Wang X, Guo H, Feng D, *et al*. Pterostilbene Attenuates Astrocytic Inflammation and Neuronal Oxidative Injury After Ischemia-Reperfusion by Inhibiting NF-κB Phosphorylation. Frontiers in Immunology. 2019; 10: 2408. https://doi.org/10.3389/fimmu.2019.02408.